Muon capture on ^{3}H

J. Golak, R. Skibiński, H. Witała, and K. Topolnicki
M. Smoluchowski Institute of Physics, Jagiellonian University, PL-30384 Kraków, Poland

H. Kamada
Department of Physics, Faculty of Engineering, Kyushu Institute of Technology, Kitakyushu 804-8550, Japan

A. Nogga
Institut für Kernphysik (Theorie), Institute for Advanced Simulation, Jülich Center for Hadron Physics and JARA-High Performance Computing, Forschungszentrum Jülich, D-52425 Jülich, Germany

L. E. Marcucci
Department of Physics, University of Pisa, IT-56127 Pisa, Italy, and INFN-Pisa, IT-56127 Pisa, Italy
(Received 19 May 2016; published 14 September 2016)

The $\mu^- + {}^3\mathrm{H} \to \nu_\mu + n + n + n$ capture reaction is studied under full inclusion of final-state interactions. Predictions for the three-body breakup of ^{3}H are calculated with the AV18 potential, augmented by the Urbana IX three-nucleon force. Our results are based on the single-nucleon weak-current operator comprising the dominant relativistic corrections. This work is a natural extension of our investigations of the $\mu^- + {}^3\mathrm{He} \to \nu_\mu + {}^3\mathrm{H}$, $\mu^- + {}^3\mathrm{He} \to \nu_\mu + n + d$ and $\mu^- + {}^3\mathrm{He} \to \nu_\mu + n + n + p$ capture reactions presented in Golak *et al.* [J. Golak, R. Skibiński, H. Witała, K. Topolnicki, A. E. Elmeshneb, H. Kamada, A. Nogga, and L. E. Marcucci, Phys. Rev. C **90**, 024001 (2014)].

DOI: 10.1103/PhysRevC.94.034002

I. INTRODUCTION

Muon capture reactions on light nuclei have been studied intensively, both experimentally and theoretically, for many years. Earlier achievements are summarized in Refs. [1–3]. More recent theoretical work has focused on the $\mu^- + {}^2\mathrm{H} \to \nu_\mu + n + n$ and $\mu^- + {}^3\mathrm{He} \to \nu_\mu + {}^3\mathrm{H}$ reactions and is described in Refs. [4–6]. The calculation of Ref. [4] was performed both in the phenomenological and the "hybrid" chiral effective field theory (χEFT) approach, initiated in Ref. [7]. It was based on Hamiltonians comprising two-nucleon (2N) and three-nucleon (3N) potentials. The weak-current operator included not only the single-nucleon contribution but also meson-exchange currents (MECs) as well as currents arising from the Δ-isobar excitation [8]. Later these two reactions were studied in a "nonhybrid" χEFT approach [9,10], where both potentials and currents were derived consistently from χEFT. The results obtained within different approaches agree with each other and describe the available experimental data well.

In Ref. [11] we joined our expertise: from the momentum space treatment of electromagnetic processes [12,13] and from the potential model approach developed in Ref. [4]. We found that new results for the $\mu^- + {}^2\mathrm{H} \to \nu_\mu + n + n$ and $\mu^- + {}^3\mathrm{He} \to \nu_\mu + {}^3\mathrm{H}$ reactions calculated in the momentum space were in good agreement with those of Ref. [4], which had been obtained using the hyperspherical harmonics formalism. Thus we could take the first step to establish a theoretical framework that can be extended to all the $A \leqslant 3$ muon capture reactions, including three-body breakup of the $A = 3$ systems. By using the Faddeev equation approach, we provided, for the first time, predictions for the total and differential capture rates of the $\mu^- + {}^3\mathrm{He} \to \nu_\mu + n + d$ and $\mu^- + {}^3\mathrm{He} \to \nu_\mu + n + p$ breakup reactions, calculated with the full inclusion of final-state 2N and 3N interactions. Although we incorporated selected MECs in the momentum space treatment of the $\mu^- + {}^2\mathrm{H} \to \nu_\mu + n + n$ and $\mu^- + {}^3\mathrm{He} \to \nu_\mu + {}^3\mathrm{H}$ capture reactions, in the calculations of the breakup channels in muon capture on ^{3}He we restricted ourselves to the single-nucleon current, with the weak nucleon form factors from Ref. [14].

Muon capture on ^{3}H has attracted less attention. This reaction, with all uncharged particles in the final state, would be very difficult to measure because of the radioactivity of the target and due to the mesomolecular complications [1]. The $\mu^- + {}^3\mathrm{H} \to \nu_\mu + n + n + n$ capture process presents, however, interesting features that make this process worth investigating: it allows one to study the neutron-neutron interaction and the three-neutron force acting exclusively in the total isospin $T = 3/2$ state. Moreover, its study is the natural next step after the $\mu^- + {}^3\mathrm{He} \to \nu_\mu + n + n + p$ reaction has been considered. Theoretical studies of muon capture on ^{3}H were started in the 1970s [15–17]. Those early calculations were performed predominantly in configuration space, using the 2N potential models available at that time. In Ref. [15] a separable potential of the Yamaguchi type was employed in the calculations based on Amado's method [18] and thus the final-state interaction (FSI) was taken into account. Actually that article focused on the three different muon capture reactions in ^{3}He and the information about the capture rate on ^{3}H was extracted from the total isospin $T = 3/2$ rate calculated for the three-body breakup of ^{3}He. The FSI effects and meson-exchange currents were neglected in Ref. [16] but some observations about the reaction mechanism proved to be correct. In particular the authors predicted that inclusion of the FSI would lead to an enhancement of the muon capture rate. A better calculation scheme was introduced in

Ref. [17]. The authors presented a general method to deal with transitions from a 3N bound state to scattering states caused by a weakly acting Hamiltonian and applied it to muon capture on ^{3}H. They obtained results not only under the plane wave (PW) approximation but also including 2N interactions (in the form of the supersoft-core nucleon-nucleon potential [19]) in the three-neutron continuum. More recent theoretical investigations were conducted by Dzhibuti and Kezerashvili [20]; they used the method of hyperspherical functions in coordinate space and employed four different central potentials in their calculations. Like in Ref. [17], they found FSI effects to be very important. Their results were sensitive to the form of the 2N potential used in the calculations. Table I in Ref. [20] nicely summarized all the early theoretical predictions.

In this article we extend our investigations of the $\mu^- + {}^3\mathrm{He} \to \nu_\mu + n + d$ and $\mu^- + {}^3\mathrm{He} \to \nu_\mu + n + n + p$ capture reactions presented in Ref. [11] to describe also the $\mu^- + {}^3\mathrm{H} \to \nu_\mu + n + n + n$ process. This reaction is studied under full inclusion of final-state interactions, employing the AV18 2N potential [21] alone or together with the Urbana IX 3N force [22]. Our results are based on the single-nucleon weak-current operator including relativistic corrections [11].

In principle the total capture rates on ^{3}H and ^{3}He in the full breakup channel for the total 3N isospin $T = 3/2$ are related by an isospin transformation. Therefore, we could use results given already in Ref. [11]. A similar situation was found for the response functions in inclusive electron scattering on ^{3}H and ^{3}He (see, for example, Refs. [12,23]). The isospin relation holds exactly if one assumes that the proton-neutron or (strong) proton-proton interactions are the same. Nowadays it seems rather indispensable to take the charge independence breaking, at least on the level of 2N interactions, into account. We do not think that using only the proton-neutron 2N potential in the study of the total muon capture rate on ^{3}He would have made a big difference but we included the neutron-neutron (and proton-proton) interactions in the 3N continuum to be consistent with the 3N bound-state calculations. Because presently our calculations do not require large computational resources, we can afford new calculations including different 2N interactions and do not rely on the isospin relation. Moreover, we follow the historical path and get the total capture rate by explicit integrations over the whole three-neutron phase space, which allows us to show also differential capture rates. This information could be potentially useful for benchmark calculations and (hopefully) for future experimental studies.

The article is organized in the following way. In Sec. II we briefly introduce the elements of our formalism. Our main results are shown in Sec. III, where we discuss various predictions obtained with different dynamics for the $\mu^- + {}^3\mathrm{H} \to \nu_\mu + n + n + n$ reaction. We show our results for the differential and integrated rates and compare them with earlier theoretical predictions. To the best of our knowledge, we are for the first time able to include final-state interactions based on modern 2N and 3N forces in a manner consistent with the bound-state calculations. In all cases we show separate results for the capture rates from the two hyperfine states, $F = 0$ and $F = 1$, of the muon-tritium atom. Finally, Sec. IV contains concluding remarks.

II. THEORETICAL FORMALISM

For the muon capture process one assumes that the initial state $|i\rangle$ consists of the atomic K-shell muon wave function $|\psi m_\mu\rangle$ with the muon spin projection m_μ and the initial nucleus state with the three-momentum $\mathbf{P}_i$ (and the spin projection m_i):

$$|i\rangle = |\psi m_\mu\rangle |\Psi_i \mathbf{P}_i m_i\rangle. \tag{2.1}$$

In the final state, $|f\rangle$, one encounters the muon neutrino (with the three-momentum $\mathbf{p}_\nu$ and the spin projection m_ν), as well as the final nuclear state with the total three-momentum $\mathbf{P}_f$ and the set of spin projections m_f:

$$|f\rangle = |\nu_\mu \mathbf{p}_\nu m_\nu\rangle\, |\Psi_f \mathbf{P}_f m_f\rangle. \tag{2.2}$$

The transition from the initial to the final state is driven by the Fermi form of the interaction Lagrangian (see, for example, Ref. [24]) and leads to a contraction of the leptonic ($\mathcal{L}_\lambda$) and nuclear ($\mathcal{N}^\lambda$) parts in the S-matrix element S_{fi} [25]:

$$S_{fi} = i(2\pi)^4 \delta^4(P' - P) \frac{G}{\sqrt{2}} \mathcal{L}_\lambda \mathcal{N}^\lambda, \tag{2.3}$$

where $G = 1.149\,39 \times 10^{-5}$ GeV^{-2} is the Fermi constant (taken from Ref. [4]) and P (P') is the total initial (final) four-momentum. The well-known leptonic matrix element

$$\mathcal{L}_\lambda = \frac{1}{(2\pi)^3} \bar{u}(\mathbf{p}_\nu, m_\nu) \gamma_\lambda (1 - \gamma_5) u(\mathbf{p}_\mu, m_\mu) \equiv \frac{1}{(2\pi)^3} L_\lambda \tag{2.4}$$

is given in terms of the Dirac matrices and spinors.

The nuclear part is the essential ingredient of the formalism and is written as [12,25]

$$\mathcal{N}^\lambda = \frac{1}{(2\pi)^3} \langle \Psi_f \mathbf{P}_f m_f | j_w^\lambda | \Psi_i \mathbf{P}_i m_i \rangle \equiv \frac{1}{(2\pi)^3} N^\lambda. \tag{2.5}$$

It is a matrix element of the nuclear weak-current operator j_w^λ between the initial and final nuclear states. In this article we omit many-nucleon contributions to j_w^λ and restrict ourselves to two forms of the single-nucleon current operator. The first one, $j_w^\lambda = j_{\mathrm{NR}}^\lambda$, is strictly nonrelativistic, with the following momentum-space matrix elements of its time and space components [25]:

$$\langle \mathbf{p}' | j_{\mathrm{NR}}^0 | \mathbf{p} \rangle = \left(g_1^V + g_1^A \frac{\boldsymbol{\sigma} \cdot (\mathbf{p} + \mathbf{p}')}{2M} \right) \tau_- \tag{2.6}$$

and

$$\begin{aligned} &\langle \mathbf{p}' | \mathbf{j}_{\mathrm{NR}} | \mathbf{p} \rangle \\ &= \left(g_1^V \frac{\mathbf{p} + \mathbf{p}'}{2M} - \frac{1}{2M} \left(g_1^V - 2M g_2^V \right) i\boldsymbol{\sigma} \times (\mathbf{p} - \mathbf{p}') \right. \\ &\quad \left. + g_1^A \boldsymbol{\sigma} + g_2^A (\mathbf{p} - \mathbf{p}') \frac{\boldsymbol{\sigma} \cdot (\mathbf{p} - \mathbf{p}')}{2M} \right) \tau_-, \end{aligned} \tag{2.7}$$

where M is the mean value of the proton (M_p) and neutron (M_n) masses, $M \equiv \frac{1}{2}(M_p + M_n)$, $\tau_- \equiv (\tau_x - i\tau_y)/2$ is the

isospin lowering operator, $\boldsymbol{\sigma}$ is a vector of Pauli spin matrices, and $\mathbf{p}$ ($\mathbf{p}'$) is the initial (final) nucleon momentum. Here we keep only terms up to $1/M$.

The second form of j^{λ}_{w}, $j^{\lambda}_{\mathrm{NR+RC}}$, contains relativistic $1/M^2$ corrections, which leads to additional terms in the corresponding matrix elements [11]:

$$\langle \mathbf{p}'|j^{0}_{\mathrm{NR+RC}}|\mathbf{p}\rangle = \Big(g_1^V - \big(g_1^V - 4Mg_2^V\big)\frac{(\mathbf{p}'-\mathbf{p})^2}{8M^2} + \big(g_1^V - 4Mg_2^V\big)i\,\frac{(\mathbf{p}'\times\mathbf{p})\cdot\boldsymbol{\sigma}}{4M^2} + g_1^A\frac{\boldsymbol{\sigma}\cdot(\mathbf{p}+\mathbf{p}')}{2M} + g_2^A\frac{(\mathbf{p}'^2-\mathbf{p}^2)}{4M^2}\boldsymbol{\sigma}\cdot(\mathbf{p}'-\mathbf{p})\Big)\tau_- \tag{2.8}$$

and

$$\langle \mathbf{p}'|\mathbf{j}_{\mathrm{NR+RC}}|\mathbf{p}\rangle = \Big[g_1^V\frac{\mathbf{p}+\mathbf{p}'}{2M} - \frac{1}{2M}\big(g_1^V - 2Mg_2^V\big)i\boldsymbol{\sigma}\times(\mathbf{p}-\mathbf{p}') + g_1^A\Big(1-\frac{(\mathbf{p}+\mathbf{p}')^2}{8M^2}\Big)\boldsymbol{\sigma} + \frac{g_1^A}{4M^2}[(\mathbf{p}\cdot\boldsymbol{\sigma})\mathbf{p}' + (\mathbf{p}'\cdot\boldsymbol{\sigma})\mathbf{p} + i(\mathbf{p}\times\mathbf{p}')] + g_2^A(\mathbf{p}-\mathbf{p}')\frac{\boldsymbol{\sigma}\cdot(\mathbf{p}-\mathbf{p}')}{2M}\Big]\tau_-. \tag{2.9}$$

This form of the nuclear weak-current operator is very close to the one used in Ref. [4]; see Ref. [11] for details. Note that the weak nucleon form factors g_1^V, g_2^V, g_1^A, and g_2^A are usually expressed in terms of the isovector components of the electric (G_E^V) and magnetic (G_M^V) Sachs form factors as well as the axial (G_A) and pseudoscalar (G_P) form factors:

$$G_E^V = g_1^V, \tag{2.10}$$

$$G_M^V = g_1^V - 2Mg_2^V, \tag{2.11}$$

$$G_A = -g_1^A, \tag{2.12}$$

$$G_P = -g_2^A m_\mu. \tag{2.13}$$

Like in Ref. [11], in this article we also employ the form factors from Ref. [14].

The essential part of the decay rate formula stems from the contraction of the leptonic and nuclear matrix elements. Note that, contrary to what was erroneously stated in Ref. [11], we use indeed the same notation as Bjorken and Drell [26] but with the different spinor normalization. To be explicit, we use the following definitions:

$$u(\mathbf{p},s) \equiv \sqrt{\frac{E+m}{2\,E}}\begin{pmatrix}\chi_s\\ \frac{\mathbf{p}\cdot\boldsymbol{\sigma}}{E+m}\chi_s\end{pmatrix}, \tag{2.14}$$

which means that $u^\dagger u = 1$ and $\bar{u}u = \frac{m}{E}$, where m is the particle mass and $E \equiv \sqrt{m^2+\mathbf{p}^2}$. We assume of course that the two-component spinor χ_s is normalized to yield $\chi_s^\dagger\chi_s = 1$.

Because we deal with a specific muon capture reaction, we switch from the general notation to the one where the relevant spin projections are given explicitly:

$$L_\lambda \equiv L_\lambda(m_\nu,m_\mu),$$
$$N^\lambda \equiv N^\lambda(m_1,m_2,m_3,m_{^3\mathrm{H}}), \tag{2.15}$$

and we use in the following the minus one spherical component of $\mathbf{N}$: $N_{-1} = \frac{1}{\sqrt{2}}(N_x - iN_y)$. With these definitions, assuming additionally that $\hat{\mathbf{p}}_\nu = -\hat{\mathbf{z}}$ and that the initial muon is at rest, we easily evaluate the following for the unpolarized case:

$$\begin{aligned}|\mathcal{T}|^2 &\equiv \frac{1}{4}\sum_{m_{^3\mathrm{H}},m_\mu}\sum_{m_1,m_2,m_3,m_\nu}|L_\lambda(m_\nu,m_\mu)N^\lambda(m_1,m_2,m_3,m_{^3\mathrm{H}})|^2\\ &= \frac{1}{2}\sum_{m_{^3\mathrm{H}}}\sum_{m_1,m_2,m_3}(|N^0(m_1,m_2,m_3,m_{^3\mathrm{H}})|^2 + |N_z(m_1,m_2,m_3,m_{^3\mathrm{H}})|^2\\ &\quad + 2|N_{-1}(m_1,m_2,m_3,m_{^3\mathrm{H}})|^2 + 2\mathrm{Re}\{N^0(m_1,m_2,m_3,m_{^3\mathrm{H}})[N_z(m_1,m_2,m_3,m_{^3\mathrm{H}})]^*\}).\end{aligned} \tag{2.16}$$

This form is not appropriate when we want to separately calculate capture rates from two hyperfine states, $F = 0$ or $F = 1$, of the muon-tritium atom. In such a case we introduce the coupling between the triton and muon spin via standard Clebsch-Gordan coefficients $c(\frac{1}{2},\frac{1}{2},F;m_\mu,m_{^3\mathrm{H}},m_F)$ and obtain

$$|\mathcal{T}|^2_F \equiv \frac{1}{2F+1}\sum_{m_F}\sum_{m_1,m_2,m_3,m_\nu}\Big|\sum_{m_\mu,m_{^3\mathrm{H}}}c\Big(\frac{1}{2},\frac{1}{2},F;m_\mu,m_{^3\mathrm{H}},m_F\Big)L_\lambda(m_\nu,m_\mu)N^\lambda(m_1,m_2,m_3,m_{^3\mathrm{H}})\Big|^2. \tag{2.17}$$

The explicit formulas for $F = 0$ and $F = 1$ read

$$|\mathcal{T}|^2_{F=0} = \sum_{m_1,m_2,m_3} \left| N^0\left(m_1,m_2,m_3,m_{^3\mathrm{H}} = -\frac{1}{2}\right) - \sqrt{2}N_{-1}\left(m_1,m_2,m_3,m_{^3\mathrm{H}} = \frac{1}{2}\right) + N_z\left(m_1,m_2,m_3,m_{^3\mathrm{H}} = -\frac{1}{2}\right)\right|^2 \tag{2.18}$$

and

$$\begin{aligned}
|\mathcal{T}|^2_{F=1} = \frac{2}{3}\sum_{m_1,m_2,m_3} \Bigg(& \left|N^0\left(m_1,m_2,m_3,m_{^3\mathrm{H}} = \frac{1}{2}\right)\right|^2 + 2\left|N_{-1}\left(m_1,m_2,m_3,m_{^3\mathrm{H}} = -\frac{1}{2}\right)\right|^2 \\
& + \left|N_{-1}\left(m_1,m_2,m_3,m_{^3\mathrm{H}} = \frac{1}{2}\right)\right|^2 + \frac{1}{2}\left|N^0\left(m_1,m_2,m_3,m_{^3\mathrm{H}} = -\frac{1}{2}\right) + N_z\left(m_1,m_2,m_3,m_{^3\mathrm{H}} = -\frac{1}{2}\right)\right|^2 \\
& + \left|N_z\left(m_1,m_2,m_3,m_{^3\mathrm{H}} = \frac{1}{2}\right)\right|^2 + 2\mathrm{Re}\left\{N^0\left(m_1,m_2,m_3,m_{^3\mathrm{H}} = \frac{1}{2}\right)\left[N_z\left(m_1,m_2,m_3,m_{^3\mathrm{H}} = \frac{1}{2}\right)\right]^*\right\} \\
& + \sqrt{2}\mathrm{Re}\left\{N^0\left(m_1,m_2,m_3,m_{^3\mathrm{H}} = -\frac{1}{2}\right)\left[N_{-1}\left(m_1,m_2,m_3,m_{^3\mathrm{H}} = \frac{1}{2}\right]\right)^*\right\} \\
& + \sqrt{2}\mathrm{Re}\left\{N_z\left(m_1,m_2,m_3,m_{^3\mathrm{H}} = -\frac{1}{2}\right)\left[N_{-1}\left(m_1,m_2,m_3,m_{^3\mathrm{H}} = \frac{1}{2}\right)\right]^*\right\}\Bigg).
\end{aligned} \tag{2.19}$$

These three quantities, $|\mathcal{T}|^2$, $|\mathcal{T}|^2_{F=0}$, and $|\mathcal{T}|^2_{F=1}$ are not independent but obey the obvious relation

$$|\mathcal{T}|^2 = \tfrac{1}{4}|\mathcal{T}|^2_{F=0} + \tfrac{3}{4}|\mathcal{T}|^2_{F=1}. \tag{2.20}$$

The crucial matrix elements

$$N^\lambda(m_1,m_2,m_3,m_{^3\mathrm{H}}) \equiv \langle \Psi^{(-)}_{nnn}\mathbf{P}_f = -\mathbf{p}_\nu m_1 m_2 m_3 | j^\lambda_w | \Psi_{^3\mathrm{H}} \mathbf{P}_i = 0 m_{^3\mathrm{H}}\rangle \tag{2.21}$$

are calculated in two steps [12,13]. First we solve a Faddeev-like equation for the auxiliary state $|U^\lambda\rangle$ for each considered neutrino energy:

$$\begin{aligned}
|U^\lambda\rangle = & \left[tG_0 + \tfrac{1}{2}(1+P)V_4^{(1)}G_0(1+tG_0)\right](1+P)j^\lambda_w|\Psi_{^3\mathrm{H}}\rangle \\
& + \left[tG_0P + \tfrac{1}{2}(1+P)V_4^{(1)}G_0(1+tG_0)P\right]|U^\lambda\rangle,
\end{aligned} \tag{2.22}$$

where $V_4^{(1)}$ is a part of the 3N force symmetrical under the exchange of nucleons 2 and 3, G_0 is the free 3N propagator, and t is the 2N t operator acting in the (2,3) subspace. Further, P is the permutation operator built from the transpositions P_{ij} exchanging nucleons i and j:

$$P = P_{12}P_{23} + P_{13}P_{23}. \tag{2.23}$$

In the second step the nuclear matrix elements are calculated by quadratures:

$$\begin{aligned}
& N^\lambda(m_1,m_2,m_3,m_{^3\mathrm{H}}) \\
& = \langle \phi_{nnn}\mathbf{pq}m_1m_2m_3|(1+P)j^\lambda_w|\Psi_{^3\mathrm{H}}\rangle \\
& \quad + \langle \phi_{nnn}\mathbf{pq}m_1m_2m_3|tG_0(1+P)j^\lambda_w|\Psi_{^3\mathrm{H}}\rangle \\
& \quad + \langle \phi_{nnn}\mathbf{pq}m_1m_2m_3|P|U^\lambda\rangle \\
& \quad + \langle \phi_{nnn}\mathbf{pq}m_1m_2m_3|tG_0P|U^\lambda\rangle.
\end{aligned} \tag{2.24}$$

Here $|\phi_{nnn}\mathbf{pq}m_1m_2m_3\rangle$ is a product state of Jacobi momenta $\mathbf{p}$ and $\mathbf{q}$ describing two free motions in the three-neutron system:

$$\begin{aligned}
\mathbf{p} &\equiv \tfrac{1}{2}(\mathbf{p}_2 - \mathbf{p}_3), \\
\mathbf{q} &\equiv \tfrac{2}{3}\left(\mathbf{p}_1 - \tfrac{1}{2}(\mathbf{p}_2 + \mathbf{p}_3)\right) = \mathbf{p}_1 + \frac{1}{3}\mathbf{p}_\nu.
\end{aligned} \tag{2.25}$$

Equations (2.22) and (2.24) simplify significantly when $V_4^{(1)} = 0$ [13]. In this case one obtains

$$|U^\lambda\rangle = tG_0(1+P)j^\lambda_w|\Psi_{^3\mathrm{H}}\rangle + tG_0P|U^\lambda\rangle \tag{2.26}$$

and

$$\begin{aligned}
& N^\lambda(m_1,m_2,m_3,m_{^3\mathrm{H}})\langle \phi_{nnn}\mathbf{pq}m_1m_2m_3|(1+P)j^\lambda_w|\Psi_{^3\mathrm{H}}\rangle \\
& \quad + \langle \phi_{nnn}\,\mathbf{p}\,\mathbf{q}\,m_1\,m_2\,m_3\,|\,(1+P)|U^\lambda\rangle\,.
\end{aligned} \tag{2.27}$$

Taking all factors into account, using the rotational symmetries of the unpolarized case and evaluating the phase-space factor in terms of the relative Jacobi momenta $\mathbf{p}$ and $\mathbf{q}$, we arrive at the final expression for the total capture rate for the $\mu^- + {}^3\mathrm{H} \to \nu_\mu + n + n + n$ reaction:

$$\begin{aligned}
\Gamma = & \frac{3}{2}G^2\frac{1}{(2\pi)^2}\mathcal{R}\frac{(M'_{^3\mathrm{H}}\alpha)^3}{\pi}4\pi \\
& \times \int_0^{E_\nu^{\max,nnn}} dE_\nu E_\nu^2 \frac{1}{3}\int_0^\pi d\theta_q \sin\theta_q 2\pi \int_0^\pi d\theta_p \sin\theta_p \\
& \times \int_0^{2\pi} d\phi_p \int_0^{p^{\max}} dp p^2 \frac{2}{3} M q |\mathcal{T}|^2,
\end{aligned} \tag{2.28}$$

where the factor $\frac{(M'_{^3\mathrm{H}}\alpha)^3}{\pi}$ stems from the K-shell atomic wave function, $M'_{^3\mathrm{H}} = \frac{M_{^3\mathrm{H}} M_\mu}{M_{^3\mathrm{H}} + M_\mu}$, and $\alpha \approx \frac{1}{137}$ is the fine-structure constant. The value of $q \equiv |\mathbf{q}|$ is defined through Eq. (2.29) below. The additional factor $\mathcal{R}$ can account for the finite volume of the ^{3}H charge but we take $\mathcal{R} = 1$ in the present

calculations. Note that the current operator of nucleon 1 is used when evaluating $|\mathcal{T}|^2$.

To fix the upper limit of the integration over p in Eq. (2.28), we express the energy conservation in terms of the Jacobi momenta:

$$M_\mu + M_{^3\mathrm{H}} \approx E_\nu + 3M + \frac{\mathbf{p}^2}{M} + \frac{3}{4}\frac{\mathbf{q}^2}{M} + \frac{1}{6}\frac{E_\nu^2}{M}. \quad (2.29)$$

Like for the $\mu^- + {}^2\mathrm{H} \to \nu_\mu + n + n$ reaction studied in Ref. [11], we can consider the hyperfine states in the muon-tritium atom, replacing $|\mathcal{T}|^2$ by $|\mathcal{T}|^2_{F=0}$ or $|\mathcal{T}|^2_{F=1}$.

III. RESULTS FOR THE $\mu^- + {}^3\mathrm{H} \to \nu_\mu + n + n + n$ REACTION

We start with the kinematics of the $\mu^- + {}^3\mathrm{H} \to \nu_\mu + n + n + n$ reaction, which is formulated exactly in the same way as in Ref. [11] for the $\mu^- + {}^3\mathrm{He} \to \nu_\mu + n + n + p$ process. The relativistic (rel) and nonrelativistic (nrl) maximal neutrino energies for this three-body capture of the muon atom are evaluated as

$$\left(E_\nu^{\max,nnn}\right)^{\mathrm{rel}} = \frac{M_{^3\mathrm{H}}{}^2 + 2M_{^3\mathrm{H}}M_\mu + M_\mu{}^2 - 9M_n{}^2}{2(M_{^3\mathrm{H}} + M_\mu)} = 94.3078\ \mathrm{MeV}, \quad (3.1)$$

$$\left(E_\nu^{\max,nnn}\right)^{\mathrm{nrl}} = \sqrt{3M_n\,(2M_{^3\mathrm{H}} + 2M_\mu - 3M_n)} - 3M_n = 94.3073\ \mathrm{MeV}. \quad (3.2)$$

The kinematically allowed region in the E_ν-E_n plane for the breakup of ^{3}H is shown in Fig. 1. We show the curves based on the relativistic and nonrelativistic kinematics. They essentially overlap except for very small neutrino energies. Up to a certain E_ν value, which we denote by $E_\nu^{2\mathrm{sol}}$, the minimal neutron kinetic energy is zero. The minimal neutron kinetic energy is greater than zero for $E_\nu > E_\nu^{2\mathrm{sol}}$. Even this very detailed feature of the kinematical domain can be calculated nonrelativistically with high accuracy (see also the inset in Fig. 1). The values of $E_\nu^{2\mathrm{sol}}$ based on the relativistic kinematics,

$$\left(E_\nu^{2\mathrm{sol}}\right)^{\mathrm{rel}} = \frac{(M_{^3\mathrm{H}} + M_\mu)(M_{^3\mathrm{H}} + M_\mu - 2M_n) - 3M_n{}^2}{2(M_{^3\mathrm{H}} + M_\mu - M_n)}, \quad (3.3)$$

and nonrelativistic kinematics,

$$\left(E_\nu^{2\mathrm{sol}}\right)^{\mathrm{nrl}} = 2\left(\sqrt{M_{^3\mathrm{H}}M_n + M_\mu M_n - 2M_n{}^2} - M_n\right), \quad (3.4)$$

yield very similar numerical values, 93.5574 and 93.5561 MeV, respectively. This supports the notion that predictions based on the nonrelativistic 3N dynamics should be valid for the considered capture process.

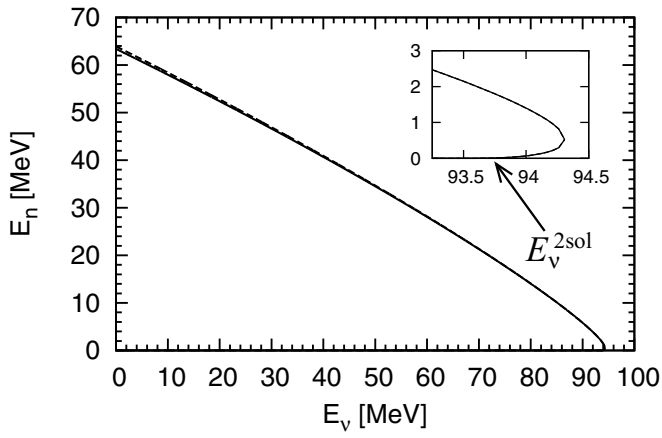

FIG. 1. The kinematically allowed region in the E_ν-E_n plane calculated relativistically (solid curve) and nonrelativistically (dashed curve) for the $\mu^- + {}^3\mathrm{H} \to \nu_\mu + n + n + n$ process.

The solutions of Eqs. (2.22) and (2.26) as well as the evaluations of the nuclear matrix elements in Eqs. (2.24) and in Eqs. (2.27) are obtained using partial-wave decomposition (PWD). We employ our standard 3N basis $|pq\bar{\alpha}\,Jm_J;Tm_T\rangle$ [12], where p and q are magnitudes of the relative Jacobi momenta and $\bar{\alpha}$ is a set of discrete quantum numbers. Note that the $|pq\bar{\alpha}Jm_J;Tm_T\rangle$ states are already antisymmetrized in the (2,3) subsystem. The initial 3N bound state is therefore represented as

$$|\Psi_{^3\mathrm{H}}m_{^3\mathrm{H}}\rangle = \sum_{\bar{\alpha}_b}\int dpp^2\int dqq^2\left|pq\bar{\alpha}_b\tfrac{1}{2}m_{^3\mathrm{H}};\tfrac{1}{2},-\tfrac{1}{2}\right\rangle \times \phi_{\bar{\alpha}_b}(p,q). \quad (3.5)$$

In our calculation of the 3N bound state we use 34 (20) points for integration over p (q) and 34 partial-wave states corresponding to the 2N subsystem total angular momentum $j \leqslant 4$.

In Ref. [11] we checked that it is sufficient to perform calculations in the 3N continuum with $j \leqslant 3$. The convergence with respect to the total 3N angular momentum J is also very rapid and in the present calculations we include all the 3N partial-wave states up to $J_{\max} = \frac{9}{2}$. The first building block in our scheme requires PWD of the single-nucleon current operator:

$$\langle pq\bar{\alpha}Jm_J;Tm_T\mathbf{P}_f|j_w(1)|\Psi_{^3\mathrm{H}}\mathbf{P}_i = 0m_{^3\mathrm{H}}\rangle. \quad (3.6)$$

This step is described in detail in Ref. [11].

We refer the reader to Ref. [12] for the detailed definitions of various 3N dynamics. Here we only note that our PW predictions shown in the following for the sake of comparison with the earlier calculations are obtained with

$$N^\lambda(m_1,m_2,m_3,m_{^3\mathrm{H}}) = \langle\phi_{nnn}\mathbf{pq}m_1m_2m_3|(1+P)j_w^\lambda|\Psi_{^3\mathrm{H}}\rangle. \quad (3.7)$$

We start the discussion of our predictions with Fig. 2, where the differential capture rates $d\Gamma/dE_\nu$ are shown for the considered $\mu^- + {}^3\mathrm{H} \to \nu_\mu + n + n + n$ capture reaction and effects of the relativistic corrections in the single-nucleon current operator are studied. The results are calculated with the 2N forces only. Although the rates are not independent [see Eq. (2.20)], we display all three quantities. Clearly, the values for $F = 0$ are much bigger than those for $F = 1$. Because the $F = 0$ rate dominates, the $F = 0$ [Fig. 2(a)] and total [Fig. 2(c)] rates change with the neutrino energy in a very similar way. They rise very slowly for small neutrino energies

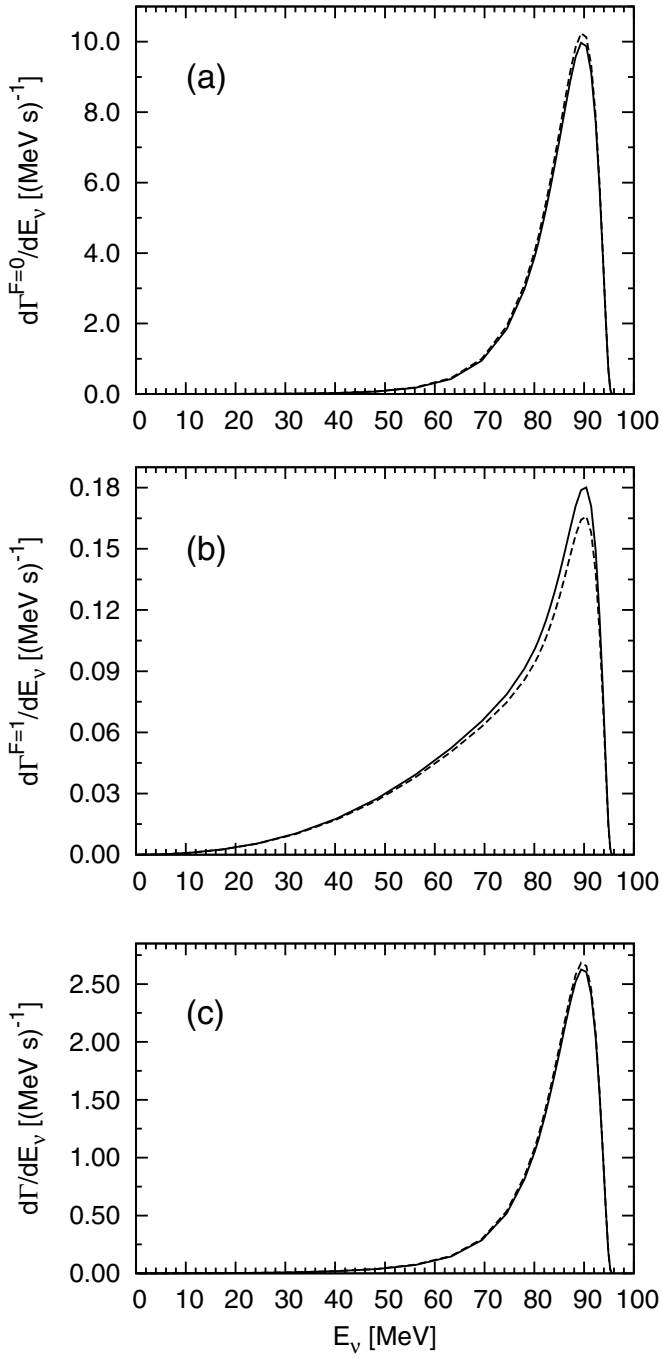

FIG. 2. The differential capture rates ($F = 0$) $d\Gamma^{F=0}/dE_\nu$ (a), ($F = 1$) $d\Gamma^{F=1}/dE_\nu$ (b), and (total) $d\Gamma/dE_\nu$ (c) for the $\mu^- + {}^3\mathrm{H} \to \nu_\mu + n + n + n$ process calculated with the single-nucleon current operator without (dashed line) and with (solid line) relativistic corrections. The calculations are based on the AV18 nucleon-nucleon potential [21] only.

and show a strong maximum in the vicinity of the maximal neutrino energy, where the phase-space factor reduces all the differential rates to zero. The behavior of the $F = 1$ rate is different. Its values grow much faster with the neutrino energy and the corresponding maximum is therefore very broad, reaching quite small neutrino energies. The relativistic effects are hardly visible on the linear scale, except for the very peak area, where two curves stop overlapping. The relativistic effects reduce the maximal values of the $F = 0$ rate (by approximately 4%) and the total rate (by approximately 2%) and increase the value of the $F = 1$ rate (by nearly 9%). The changes of the total (integrated) rates are discussed below.

Of course, a simple comparison of results based on the NR and NR + RC prescriptions for the single-nucleon current operator is not sufficient to account for all relativistic effects. Further relativistic features may be present in the data to which the nucleon weak form factors are fitted based on the fully relativistic formula, given for example by Eq. (2.6) in Ref. [11]. In principle, this relativistic formula could be used in momentum space calculations but then clearly the problem of consistence would emerge. So we apply the popular NR + RC prescription, which should actually do a good job for the studied capture reaction. Here, contrary to many kinematics considered in electron scattering on ^{3}He, the magnitude of the three-momentum transfer is smaller than 100 MeV/c, which suggests that $1/M^2$ corrections might be a good approximation.

In Fig. 3 the same differential rates are shown but they are calculated with three different types of 3N dynamics. We display predictions obtained using the PW approximation [see Eq. (3.7)], results of the calculations that employ only 2N forces (given by the AV18 potentials [21]) to calculate the initial as well as final 3N states, and finally predictions based on a consistent treatment of the initial and final states, taking additionally a 3N force (the Urbana IX [22] potential) into account. Final-state interactions are very important. They not only change the PW predictions by a factor of 2 but also alter the shapes of the curves and their peak positions. We thus confirm the findings of Refs. [17,20] obtained with completely different frameworks and much simpler forces. Like in Ref. [11], we also study the 3N force effects. They are clearly visible in the peak areas, where the predictions including the 3N force drop by approximately 20%. These peak reductions are quite similar to the two-body and three-body breakup cases studied in Ref. [11] for muon capture on ^{3}He. In these calculations the same single-nucleon current operator including relativistic corrections is used. Note that the PW results are obtained with the initial 3N bound state calculated solely with the 2N forces.

It is interesting to trace back the origin of such large 3N force effects. To this end in Fig. 4 we display results of four different calculations with the same single-nucleon current operator. We can neglect the 3N force in both the 3N bound and scattering states, include it only in the initial state and only in the final state, and finally use it consistently in the 3N bound state and in the 3N continuum. For all the three differential rates 3N force contributions to the final three-neutron scattering state are very small and do not reach even 1%. Only the inclusion of the 3N force in the initial bound state is decisive for the calculations. Therefore in Fig. 4 we see two groups of curves, each obtained with the same initial bound state.

It is clear that quantities like the differential capture rates $d\Gamma/dE_\nu$ would be extremely hard to measure. More realistic is to expect that the capture rates $d\Gamma/dE_n$ (E_n is the final neutron

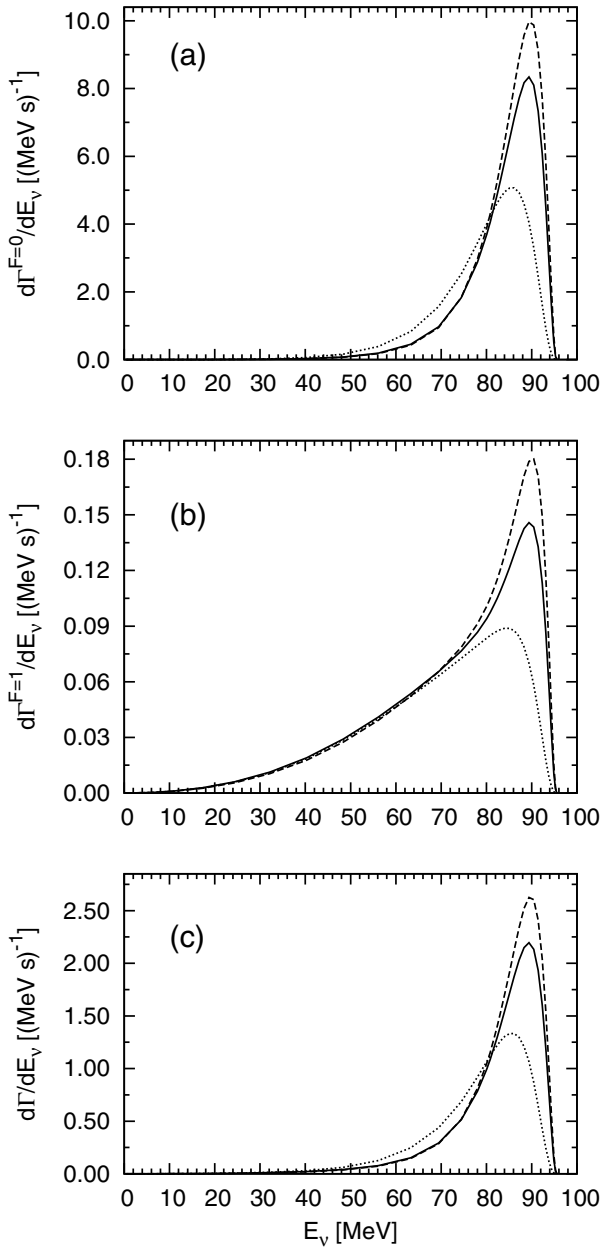

FIG. 3. The differential capture rates $(F = 0)$ $d\Gamma^{F=0}/dE_\nu$ (a), $(F = 1)$ $d\Gamma^{F=1}/dE_\nu$ (b), and (total) $d\Gamma/dE_\nu$ (c) for the $\mu^- + {}^3\mathrm{H} \to \nu_\mu + n + n + n$ process calculated with the single-nucleon current operator including relativistic corrections and different types of 3N dynamics: (symmetrized) plane wave (dotted curve), with total omission of the 3N force (dashed curve) and with consistent inclusion of the 2N and 3N forces (solid curve). The calculations are based on the AV18 nucleon-nucleon potential [21] and the Urbana IX 3N force [22].

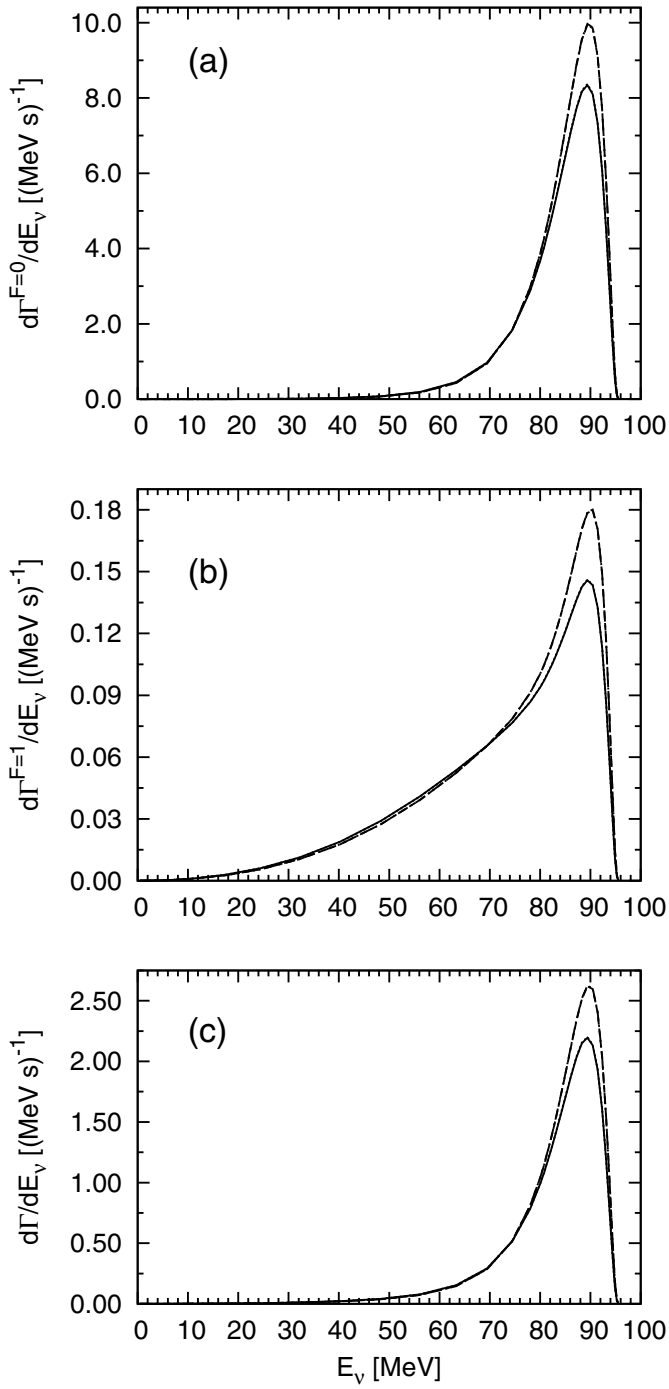

FIG. 4. The 3N force effects in the differential capture rates $(F = 0)$ $d\Gamma^{F=0}/dE_\nu$ (a), $(F = 1)$ $d\Gamma^{F=1}/dE_\nu$ (b), and (total) $d\Gamma/dE_\nu$ (c) calculated without the 3N force (dash-dotted line), including the 3N force only in the initial state (dotted line), only in the final state (dashed line), and with the 3N forces taken consistently in the initial and final states (solid line). The dash-dotted and dashed lines overlap. The same is true for the dotted and solid lines.

energy) will be accessed experimentally. Such measured rates will be in practice averaged over certain intervals of the neutron energies. To calculate the corresponding theoretical rates we do not introduce any dedicated kinematics but use the same steps as required to obtain the total rates according to Eq. (2.28). Thus we are sure that the calculations of the (averaged) differential rates $\langle d\Gamma/dE_n \rangle$ are consistent with the calculation of the total rate Γ, where we obtain first the capture rates $d\Gamma/dE_\nu$ at 36 values of the final neutrino energy, solving for each of them the corresponding Faddeev-like equation (2.22). These neutrino energies are distributed with special emphasis on the region in the vicinity of the maximal neutrino energy.

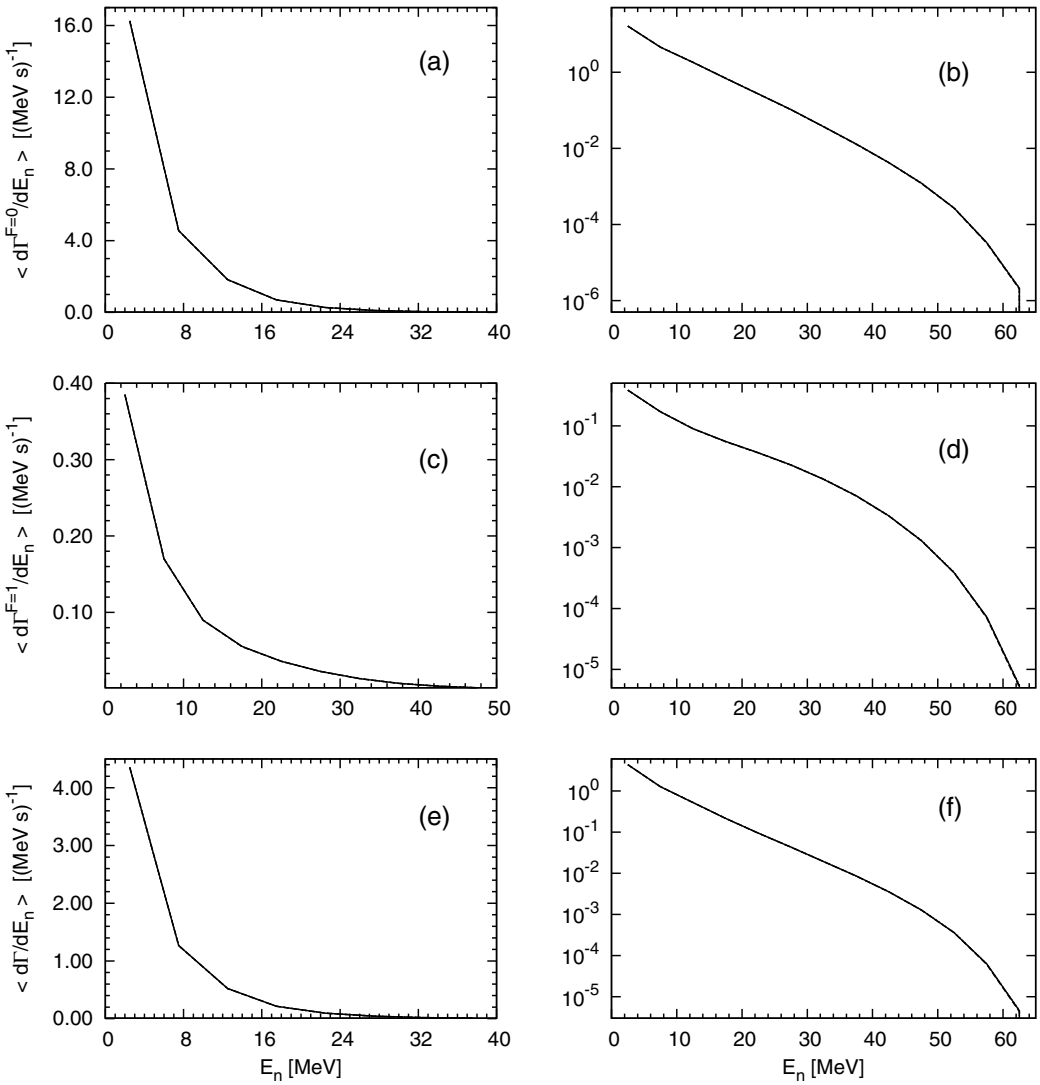

FIG. 5. The differential capture rates ($F = 0$) $\langle d\Gamma^{F=0}/dE_n\rangle$ (top panels), ($F = 1$) $\langle d\Gamma^{F=1}/dE_n\rangle$ (middle panels), and (total) $\langle d\Gamma/dE_n\rangle$ (bottom panels), for the $\mu^- + {}^3\mathrm{H} \to \nu_\mu + n + n + n$ process averaged over 5-MeV neutron energy bins. The same results are shown on a linear scale (left panels) and a logarithmic scale (right panels). The predictions are obtained using the full solution of Eq. (2.22). The three overlapping curves represent results where the energies of nucleon 1 (solid line), nucleon 2 (dashed line), and nucleon 3 (dotted line) are considered.

Therefore we use the same formulas and codes as for the total Γ capture rate, performing integrals over the whole phase space. However, the contribution to a given neutron energy interval comes only from the integrand with a proper kinematical "signature" [11].

This kinematical signature is easy to obtain because the individual momenta of the three outgoing neutrons can be evaluated from Eqs. (2.25):

$$\begin{aligned} \mathbf{p}_1 &= -\tfrac{1}{3}\mathbf{p}_\nu + \mathbf{q}, \\ \mathbf{p}_2 &= -\tfrac{1}{3}\mathbf{p}_\nu + \mathbf{p} - \tfrac{1}{2}\mathbf{q}, \\ \mathbf{p}_3 &= -\tfrac{1}{3}\mathbf{p}_\nu - \mathbf{p} - \tfrac{1}{2}\mathbf{q}. \end{aligned} \tag{3.8}$$

Because the outgoing neutrons are identical, we have actually three possibilities to calculate the final neutron energy: $E_n = \frac{1}{2M}\mathbf{p}_i^2$ ($i = 1,2,3$). This can be used as a nontrivial test of the final-state antisymmetrization.

In Fig. 5 the capture rates, $\langle d\Gamma^{F=0}/dE_n\rangle$, $\langle d\Gamma^{F=1}/dE_n\rangle$, and $\langle d\Gamma/dE_n\rangle$, averaged over 5-MeV neutron energy bins are shown on both a linear and a logarithmic scale. The reason for that is that the rates change by several orders of magnitude in the allowed interval of the neutron energy. These results are obtained with the full inclusion of the 3N force. The three curves denote the results, where the energies of nucleon 1, nucleon 2, and nucleon 3 are taken as the neutron energy E_n. The three lines completely overlap, which confirms the proper antisymmetrization of the final three-neutron states. In these calculations we use thus 36 E_ν points, 36 θ_q points, 36 θ_p points, and 36 ϕ_p points and also 36 values of the magnitude of the relative $\mathbf{p}$ momentum. Note that due to the rotational invariance of the unpolarized rate, we may choose $\phi_q = 0$. These numbers of points are sufficient to get smooth curves for the 5-MeV neutron energy bins. In Fig. 6 we show the same capture rates as in Fig. 5 but now they are averaged over smaller

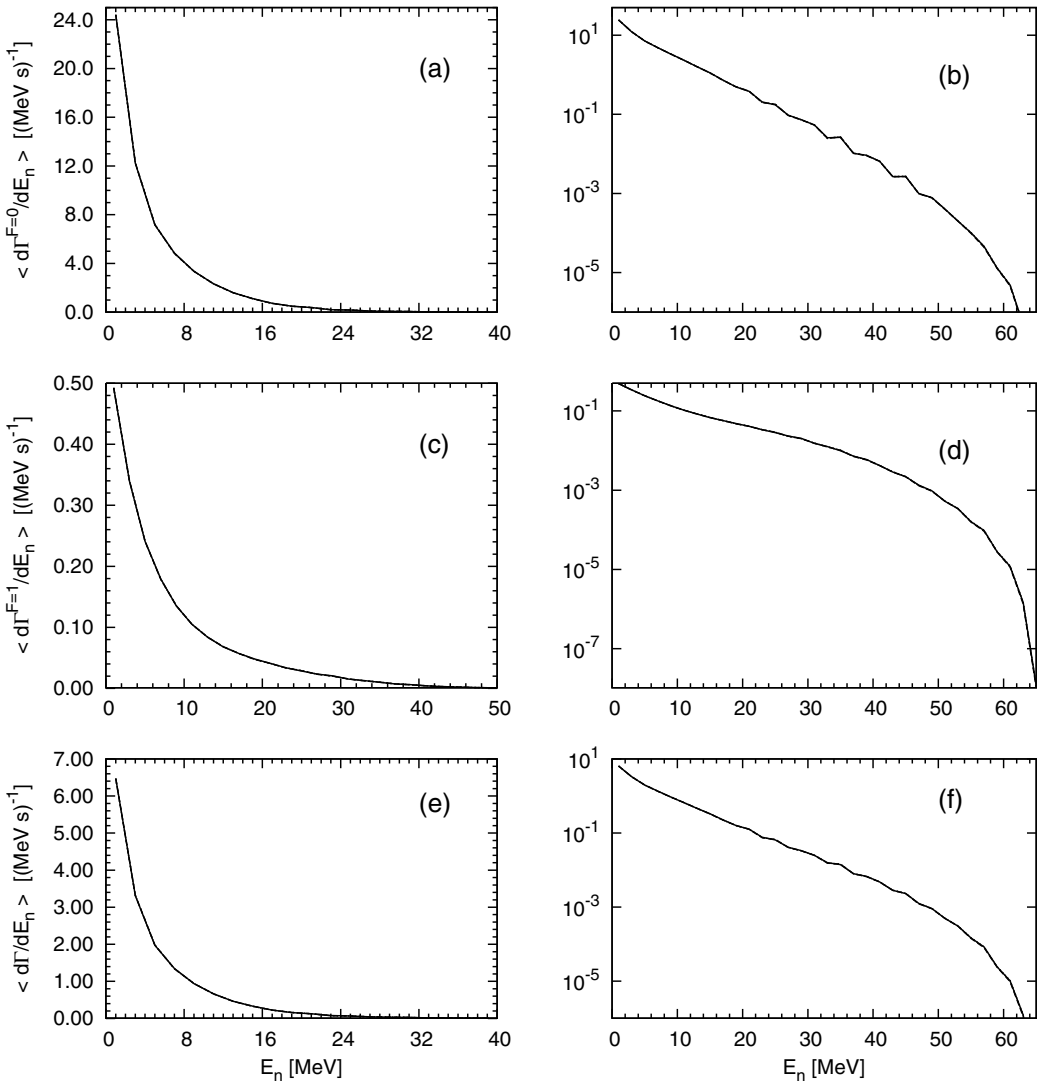

FIG. 6. The same as in Fig. 5 but the capture rates are averaged over 2-MeV neutron energy bins.

2-MeV neutron energy bins. From the wavy character of some lines (visible on the logarithmic scale) one can infer that an average over smaller than 5-MeV energy intervals requires a finer grid of E_ν points.

We supplement the results presented in Figs. 2–6 by giving the corresponding values of the integrated capture rates in Table I, together with earlier theoretical predictions of Refs. [15–17,20]. From the first two rows of this table it is clear that final-state interactions taken in the form of 2N forces enhance the plane-wave results (given in parentheses) by 34%–38%. This effect is similar for the nonrelativistic single-nucleon current operator and for the current operator containing relativistic corrections. The relativistic corrections reduce the $F = 0$ rate by approximately 3.4% and raise the $F = 1$ rate by more than 6%. The effect on the total rate is weaker: this rate is reduced by approximately 2.6%. (All these changes are discussed for the Full 2NF results.) Note that this effect is slightly larger than that for the $\mu^- + {}^3\mathrm{He} \to \nu_\mu + {}^3\mathrm{H}$ process, for which the total capture rate, calculated with the AV18 2N potential [21] augmented by the Urbana IX 3N force [22], is reduced by 1.6%, when the relativistic corrections are included in the single-nucleon current. This information was already obtained by one of the authors (L.E.M.), when the calculations published in Ref. [7] were performed, but it was not included in the publication. The inclusion of the 3N force decreases all three rates. This reduction is stronger for the $F = 0$ and total rates (approximately 12%) than for the $F = 1$ rate (approximately 7.5%). The reduction due to the 3N force is a common feature of the muon capture on the $A = 3$ systems. Already in Ref. [7] it was shown that there is a significant correlation between the total capture rate for the $\mu^- + {}^3\mathrm{He} \to \nu_\mu + {}^3\mathrm{H}$ reaction and the $A = 3$ binding energies.

It is very interesting to notice that much earlier theoretical predictions agree quite well with our new results. This is true not only for the plane-wave results but also for the calculations that consistently used 2N forces in the initial and final 3N states.

Results of our most advanced approach (the AV18 nucleon-nucleon potential augmented by the Urbana IX 3N force and the single-nucleon current operator containing relativistic

TABLE I. Capture rates (Γ) for the $\mu^- + {}^3\mathrm{H} \to \nu_\mu + n + n + n$ process calculated with the AV18 [21] nucleon-nucleon potential and the nonrelativistic single-nucleon current operator (Full 2NF), including relativistic corrections in the single-nucleon current operator (Full 2NF RC) and additionally employing the Urbana IX [22] 3N force (Full 2NF + 3NF RC). Also predictions obtained using the plane-wave approximation are shown in parentheses. Earlier theoretical predictions, obtained without a 3N force, are displayed in the same way. For the information about the various 2N forces (YAM, RSC, SSC, V, EH, S1, and S2) used in Refs. [15–17,20] we refer the reader to the corresponding articles.

	Capture rate Γ in s^{-1}		
	$F=0$	$F=1$	Total
Full 2NF	138.1 (100.0)	3.97 (2.97)	37.5 (27.2)
Full 2NF RC	133.6 (97.0)	4.21 (3.12)	36.5 (26.6)
Full 2NF + 3NF RC	118.7	3.92	32.6
Earlier theoretical predictions:			
Ref. [15] YAM			9.5 (6.1)
Ref. [16] RSC			(23.6)
RSC RC			(28.2)
SSC			(23.0)
SSC RC			(27.6)
Ref. [17] SSC	122.8 (90.6)	3.58 (2.69)	33.4 (24.7)
SSC RC	137.5 (102.0)	3.66 (2.78)	37.1 (27.6)
Ref. [20] V			35.7 (22.3)
EH			29.9 (19.7)
S1			33.1 (20.8)
S2			35.5 (21.9)

corrections) are given in the third row of Table I and read $\Gamma^{F=0} = 118.7\ \mathrm{s}^{-1}$, $\Gamma^{F=1} = 3.92\ \mathrm{s}^{-1}$, and $\Gamma = 32.6\ \mathrm{s}^{-1}$.

IV. SUMMARY AND CONCLUSIONS

This article constitutes an important step towards a consistent framework for calculations of all muon capture processes on the deuteron and $A = 3$ nuclei. This requires that the initial and final nuclear states are calculated with the same Hamiltonian and that the weak-current operator is fully consistent with the nuclear forces. Results of such calculations can be then compared with precise experimental data to improve our understanding of muon capture and other weak reactions.

In the present article we study the $\mu^- + {}^3\mathrm{H} \to \nu_\mu + n + n + n$ process in the framework close to the potential model approach of Ref. [4] but with the single-nucleon current operator. This is a continuation of our work from Ref. [11], where other capture reactions, $\mu^- + {}^2\mathrm{H} \to \nu_\mu + n + n$, $\mu^- + {}^3\mathrm{He} \to \nu_\mu + {}^3\mathrm{H}$, $\mu^- + {}^3\mathrm{He} \to \nu_\mu + n + d$, and $\mu^- + {}^3\mathrm{He} \to \nu_\mu + n + n + p$, were described in the same momentum space framework. We use the results of Ref. [11] on the partial-wave decomposition of the single-nucleon current operator, the number of partial wave states necessary to reach convergence of the results, and the simple method to obtain the averaged capture rates from the calculations of the total rate. It is quite understandable that also for this reaction the nonrelativistic kinematics can be safely used.

Using for the first time modern semiphenomenological 2N and 3N forces, we give predictions for the differential $d\Gamma/dE_\nu$ capture rates as well as for the corresponding integrated capture rates Γ and the averaged $\langle d\Gamma/dE_n \rangle$ capture rates, taking additionally into account the $F = 0$ and $F = 1$ hyperfine states of the muon-tritium atom. Our best numbers (from the calculations employing the AV18 2N potential and the Urbana IX 3N force and using the single-nucleon current operator containing relativistic corrections) are $\Gamma^{F=0} = 118.7\ \mathrm{s}^{-1}$, $\Gamma^{F=1} = 3.92\ \mathrm{s}^{-1}$, and $\Gamma = 32.6\ \mathrm{s}^{-1}$.

Our predictions obtained with the 2N force alone are in a rather good agreement with much older theoretical predictions from Refs. [15–17,20]. Our results cannot be confronted with experimental data at the moment. It is clear that a measurement of the reaction considered in this article would be extremely difficult. However, due to the presence of three neutrons in the final state and their two- and three-body interactions, theoretical and experimental investigations of this reaction are very interesting and important.

We are well aware that the full understanding of the muon capture processes requires the inclusion of at least 2N contributions to the nuclear current operators. First steps in this direction were made in Ref. [11]. We do hope that, even in the present shape, our predictions will serve as an important benchmark. In the near future we plan to perform more complete calculations using the locally regularized chiral 2N potential [27,28], supplemented by the consistently regularized chiral 3N forces [29,30] and electroweak-current operators [31].

ACKNOWLEDGMENTS

This study was supported by the Polish National Science Center under Grants No. DEC-2013/10/M/ST2/00420 and No. DEC-2013/11/N/ST2/03733. The numerical calculations were performed on the supercomputer clusters of the JSC, Jülich, Germany.

[1] D. F. Measday, Phys. Rep. **354**, 243 (2001).
[2] T. Gorringe and H. W. Fearing, Rev. Mod. Phys. **76**, 31 (2004).
[3] P. Kammel and K. Kubodera, Annu. Rev. Nucl. Part. Sci. **60**, 327 (2010).
[4] L. E. Marcucci, M. Piarulli, M. Viviani, L. Girlanda, A. Kievsky, S. Rosati, and R. Schiavilla, Phys. Rev. C **83**, 014002 (2011).
[5] L. E. Marcucci, Int. J. Mod. Phys. A **27**, 1230006 (2012).
[6] L. E. Marcucci and M. Piarulli, Few-Body Syst. **49**, 35 (2011).
[7] L. E. Marcucci, R. Schiavilla, S. Rosati, A. Kievsky, and M. Viviani, Phys. Rev. C **66**, 054003 (2002).
[8] L. E. Marcucci, R. Schiavilla, M. Viviani, A. Kievsky, S. Rosati, and J. F. Beacom, Phys. Rev. C **63**, 015801 (2000).
[9] L. E. Marcucci, A. Kievsky, S. Rosati, R. Schiavilla, and M. Viviani, Phys. Rev. Lett. **108**, 052502 (2012).
[10] L. E. Marcucci and R. Machleidt, Phys. Rev. C **90**, 054001 (2014).

[11] J. Golak, R. Skibiński, H. Witała, K. Topolnicki, A. E. Elmeshneb, H. Kamada, A. Nogga, and L. E. Marcucci, Phys. Rev. C **90**, 024001 (2014).
[12] J. Golak, R. Skibiński, H. Witała, W. Glöckle, A. Nogga, and H. Kamada, Phys. Rep. **415**, 89 (2005).
[13] R. Skibiński, J. Golak, H. Witała, W. Glöckle, and A. Nogga, Eur. Phys. J. A **24**, 31 (2005).
[14] G. Shen, L. E. Marcucci, J. Carlson, S. Gandolfi, and R. Schiavilla, Phys. Rev. C **86**, 035503 (2012).
[15] A. C. Phillips, F. Roig, and J. Ros, Nucl. Phys. A **237**, 493 (1975).
[16] J. Torre, Cl. Gignoux, and G. Goulard, Phys. Rev. Lett. **40**, 511 (1978).
[17] J. Torre and B. Goulard, Phys. Rev. Lett. **43**, 1222 (1979).
[18] R. D. Amado, Phys. Rev. **132**, 485 (1963).
[19] R. de Tourreil and D. W. L. Sprung, Nucl. Phys. A **201**, 193 (1973).
[20] R. I. Dzhibuti and R. Ya. Kezerashvili, Yad. Fiz. **39**, 1109 (1984) [Sov. J. Nucl. Phys. **39**, 700 (1984)].
[21] R. B. Wiringa, V. G. J. Stoks, and R. Schiavilla, Phys. Rev. C **51**, 38 (1995).
[22] B. S. Pudliner, V. R. Pandharipande, J. Carlson, Steven C. Pieper, and R. B. Wiringa, Phys. Rev. C **56**, 1720 (1997).
[23] J. Golak, H. Witała, H. Kamada, D. Hüber, S. Ishikawa, and W. Glöckle, Phys. Rev. C **52**, 1216 (1995).
[24] J. D. Walecka, *Theoretical Nuclear and Subnuclear Physics* (Oxford University, New York, 1995).
[25] R. Skibiński, J. Golak, H. Witała, and W. Glöckle, Phys. Rev. C **59**, 2384 (1999).
[26] J. D. Bjorken and S. D. Drell, *Relativistic Quantum Mechanics*, International Series in Pure and Applied Physics (McGraw-Hill, New York, 1998).
[27] E. Epelbaum, H. Krebs, and U.-G. Meißner, Eur. Phys. J. A **51**, 53 (2015).
[28] E. Epelbaum, H. Krebs, and U.-G. Meißner, Phys. Rev. Lett. **115**, 122301 (2015).
[29] E. Epelbaum, A. Nogga, W. Glöckle, H. Kamada, U.-G. Meißner, and H. Witała, Phys. Rev. C **66**, 064001 (2002).
[30] K. Hebeler, H. Krebs, E. Epelbaum, J. Golak, and R. Skibiński, Phys. Rev. C **91**, 044001 (2015).
[31] E. Epelbaum, H. Krebs, and U.-G. Meißner (unpublished).